

Narrow-line Cooling and Determination of Magic Wavelength of Cd

A. Yamaguchi,^{1,2} M. S. Safronova,^{3,4} K. Gibble,^{1,5} and H. Katori^{1,2,6}

¹Quantum Metrology Laboratory, RIKEN, Wako, Saitama 351-0198, Japan

²Space-Time Engineering Research Team, RIKEN, Wako, Saitama 351-0198, Japan

³Department of Physics and Astronomy, University of Delaware, Newark, Delaware 19716, USA

⁴Joint Quantum Institute, NIST and the University of Maryland, College Park, Maryland 20742, USA

⁵Department of Physics, The Pennsylvania State University, University Park, Pennsylvania 16802, USA

⁶Department of Applied Physics, Graduate School of Engineering,
The University of Tokyo, Bunkyo-ku, Tokyo 113-8656, Japan

(Dated: September 18, 2019)

We experimentally and theoretically determine the magic wavelength of the $(5s^2)^1S_0 - (5s5p)^3P_0$ clock transition of ^{111}Cd to be 419.88(14) nm and 420.1(7) nm. To perform Lamb-Dicke spectroscopy of the clock transition, we use narrow-line laser cooling on the $^1S_0 - ^3P_1$ transition to cool the atoms to 6 μK and load them into an optical lattice. Cadmium is an attractive candidate for optical lattice clocks because it has a small sensitivity to blackbody radiation and its efficient narrow-line cooling mitigates higher order light shifts. We calculate the blackbody shift, including the dynamic correction, to be fractionally $2.83(8) \times 10^{-16}$ at 300 K, an order of magnitude smaller than that of Sr and Yb. We also report calculations of the Cd 1P_1 lifetime and the ground state C_6 coefficient.

PACS numbers: 37.10.De, 32.30.-r, 34.50.-s

State-of-the-art optical atomic clocks deliver fractional accuracy and frequency stability of order 10^{-18} [1–5]. Such advanced atomic clocks motivate an optical redefinition of the second [6] and open up new applications, such as a chronometric leveling [7, 8] and laboratory searches for variations of fundamental constants [9, 10]. At this accuracy level, one of the limiting systematic uncertainties is the ac Stark shift of atomic clock transitions induced by black body radiation (BBR) [1, 3, 4]. While interrogating atoms in a cryogenic environment has successfully reduced the BBR shift in a Hg^+ clock [11], a Cs microwave clock [12], and Sr and Yb optical lattice clocks [2, 13], a number of atoms have smaller sensitivities to BBR, which can enable simpler approaches and improved accuracy. These include optical lattice clocks based on Hg, Mg, Tm, and Cd [14–19], ion clocks with Al^+ , Yb^+ , In^+ , and Lu^+ [3, 20–22], Th^{3+} nuclear clock [23, 24], and highly charged ion clocks [25, 26].

Among the candidates for optical lattice clocks, Cd is unique in having all of several desirable attributes. Two isotopes, ^{111}Cd and ^{113}Cd , both with $\gtrsim 12\%$ natural abundance, have a nuclear spin of 1/2, which precludes tensor light shifts from the lattice light and provides hyperfine-induced clock transitions with natural linewidths of $\Gamma_0/2\pi = 7.0$ mHz and 7.6 mHz [27]. Additionally, the $\lambda_2 = 326$ nm spin-forbidden $^1S_0 - ^3P_1$ transition's natural linewidth, $\Gamma_2/2\pi = 66.6$ kHz [28, 29], allows Doppler cooling to $T_{D2} = 1.58$ μK , facilitating good control of higher-order lattice light shifts [30]. The short wavelength of this near-ultraviolet narrow cooling transition also has applications beyond clocks; the small absorption cross section $3\lambda_2^2/2\pi$ reduces radiation trapping [31] and allows trapping of dense cold atomic ensembles, which may enable rapid or even continuous production of quantum degenerate gases [32–34]. A Cd clock can be

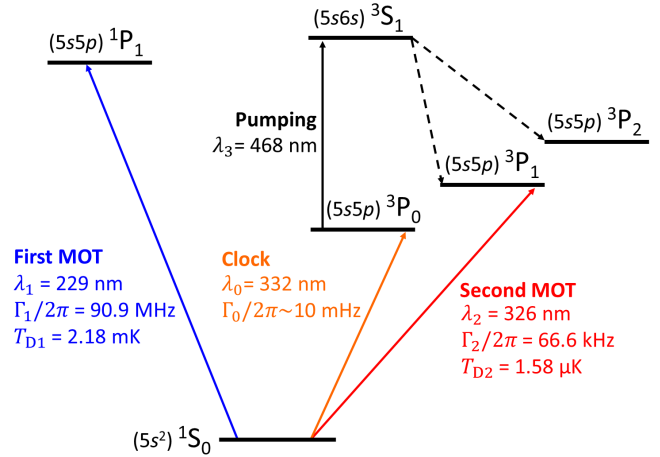


FIG. 1. Energy levels of cadmium. Wavelengths λ , natural linewidths $\Gamma/2\pi$ and, for the cooling and clock transitions, Doppler limited temperatures T_D are indicated. The magic wavelength for the optical lattice is 419.88 nm, at which the ac Stark shifts of both states of the $^1S_0 - ^3P_0$ clock transition are identical.

constructed using light for all of the transitions (Fig. 1), including the magic wavelength, made from direct, or frequency doubled or quadrupled semiconductor lasers. Along with its insensitivity to BBR, cadmium's other favorable properties permit an optical lattice clock to be accurate, compact, and portable.

Here, we demonstrate two-stage laser cooling of Cd atoms to 6 μK using the $^1S_0 - ^1P_1$ transition and the spin-forbidden $^1S_0 - ^3P_1$ transition, shown in Fig. 1. We load ultracold ^{111}Cd trapped into an optical lattice and experimentally determine the magic wavelength for the $^1S_0 - ^3P_0$ clock transition to be 419.88(14) nm, in agree-

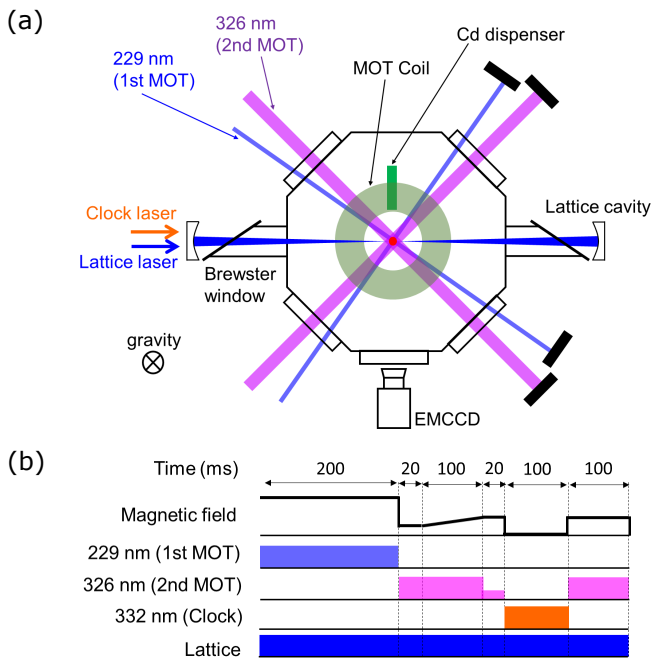


FIG. 2. (a) Cadmium clock schematic. The cooling and trapping lasers at 229 nm and 326 nm enter through anti-reflection-coated fused-silica viewports. The lattice light builds up in an enhancement cavity with fused-silica Brewster windows and external mirrors. (b) Sequence for laser cooling, spectroscopy and detection.

ment with our theoretical prediction 420.1(7) nm. Our theoretical BBR shift at 300 K is $-0.256(7)$ Hz with an extremely small dynamic correction, $-0.45(5)$ mHz. The fractional BBR shift is $2.83(8) \times 10^{-16}$ at 300 K, consistent with [35, 36], and allows 4×10^{-19} uncertainty for a temperature inaccuracy of 0.1 K.

Our experimental schematic is depicted in Fig. 2(a). A ^{111}Cd dispenser, enriched to 93%, is located 2 cm from the magneto-optical trap (MOT). We first cool and trap ^{111}Cd atoms using the $^1S_0-^1P_1$ transition, for which $\lambda_1 = 229$ nm and the natural linewidth is $\Gamma_1/2\pi = 90.9$ MHz [37]. This is referred to as the first MOT [38], which uses a magnetic field gradient of 17 mT/cm along the axis of the anti-Helmholtz coils. It uses 6 laser beams with $1/e^2$ radii of 1 mm and intensities of $0.2I_1$ for each, where $I_1 = 988$ mW/cm 2 is the saturation intensity of the transition. The total laser power for the first MOT is 30 mW, which is generated by two successive second-harmonic generation (SHG) stages [19] fed by an external cavity diode laser (ECDL) and tapered amplifier at $4\lambda_1 = 916$ nm.

Figure 2(b) shows the experimental timing sequence. Operating the first MOT for 200 ms, we typically capture 10^6 atoms. We then switch to the second MOT [39] on the narrow $\lambda_2 = 326$ nm $^1S_0-^3P_1$ transition to further cool the atoms. The laser beam $1/e^2$ radii are 2.5 mm and the total intensity of the six beams is $310I_2$,

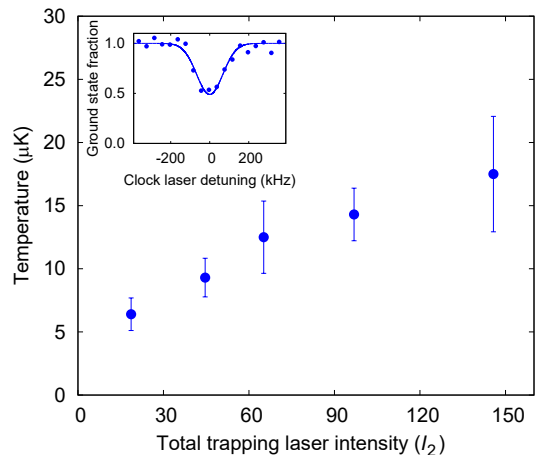


FIG. 3. Temperature of ^{111}Cd versus laser intensity for a detuning of $-3\Gamma_2$. The temperature is derived from the Doppler-broadening of the $^1S_0-^3P_0$ clock transition (see inset). A Gaussian fit (solid curve) gives a minimum temperature of 6 μK for a total intensity of $19I_2$.

with a saturation intensity $I_2 = 252$ $\mu\text{W}/\text{cm}^2$. The total laser power of 50 mW is generated by SHG of a tapered amplifier seeded by an ECDL. At the beginning of the second MOT, the magnetic field gradient is reduced to 0.1 mT/cm. To capture velocities beyond the natural linewidth Γ_2 , the laser frequency, tuned 3.965 MHz below the $^1S_0-^3P_1$ resonance, is sinusoidally modulated at 50 kHz with a peak-to-peak amplitude of 7.400 MHz by an acousto-optic modulator. After 20 ms, the magnetic field gradient increases to 0.3 mT/cm in 100 ms to make a compact cloud to efficiently load atoms into the optical lattice. In the last 20 ms, for optimum cooling, we inhibit the frequency modulation and set the detuning to $-3\Gamma_2$ and lower the intensity to $19I_2$.

Figure 3 shows the temperature of atoms from the second MOT as a function of the total laser intensity for a detuning of $-3\Gamma_2$. We measure the temperature of atoms via the Doppler broadening of the $^1S_0-^3P_0$ clock transition, as shown in the inset. The lowest temperature is 6(1) μK for an intensity of $19I_2$. At higher intensities, the atomic temperature increases, as expected for a higher heating rate from photon scattering in Doppler cooling [40].

We load ultracold Cd into a one-dimensional optical lattice in a horizontal power enhancement cavity. The cavity finesse is 200 and the $1/e^2$ beam radius is 71 μm . The lattice light, tunable around 420 nm, is made by SHG of light from a Ti:sapphire laser. The transfer efficiency from the second MOT to the lattice is about 15%, loading several thousand atoms in the lattice. The $^1S_0-^3P_0$ clock transition is excited by the clock laser propagating along the lattice axis, as shown in Fig. 2(a). The 2 mW clock laser at $\lambda_0 = 332$ nm is generated by SHG of an ECDL stabilized to a reference cavity. We

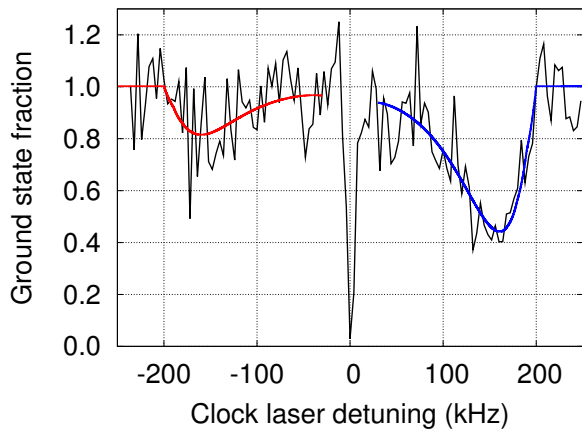


FIG. 4. Sideband spectrum of the clock transition for a lattice wavelength $\lambda_L = 419.9$ nm. The blue and red curves are fits to the blue and red motional sidebands, which determines the axial trap frequency to be 209(8) kHz.

note that the subharmonic of the Cd clock transition, $4\lambda_0 = 1328$ nm, corresponds to a telecommunication wavelength, allowing dissemination of the clock signal via telecommunication fiber networks without an optical frequency comb [7]. After applying a clock laser pulse with an intensity of 25 mW/cm² for 100 ms, the excitation is observed with electron-shelving [41], using the second MOT. The clock spectrum is detected as a decrease of the MOT fluorescence, which is measured with a 100 ms exposure on an electron-multiplying charge-coupled device (EMCCD) camera.

To measure the lattice-trap depth, the axial trap frequency is determined from the sideband spectrum of the clock transition, as shown in Fig. 4 for a lattice wavelength $\lambda_L = 419.9$ nm and peak intensity $I_L \sim 250$ kW/cm². The sideband spectra are enhanced by exciting the $^3P_0 - ^3S_1$ transition at $\lambda_3 = 468$ nm (see Fig. 1) to pump 51% of the atoms in the 3P_0 state to the 3P_2 metastable state [42]. We alternately apply 2 ms pumping and clock laser pulses, to avoid light shifts and broadening, accumulating more atoms in the 3P_2 state and further depleting the ground state. In Fig. 4, the blue and red curves are fits to the blue and red motional sidebands [43]. They yield a trap frequency of 209(8) kHz, corresponding to a lattice depth of 51(4) μ K, or 105(8) E_R , with the lattice photon recoil energy $E_R = \hbar^2/2m\lambda_L^2 = k_B \times 0.49 \mu$ K. The asymmetry of the sideband spectra in Fig. 4 indicates an atom temperature of 8(2) μ K, consistent with the Doppler broadening measurement.

To determine the magic wavelength, we measure the lattice-trap-depth dependent light shift. Figure 5(a) shows the light shift as a function of the trap depth, for six lattice wavelengths λ_L , where the trap depth is extracted from sideband spectra as in Fig. 4. For clock frequency measurements, we use a single Rabi clock pulse

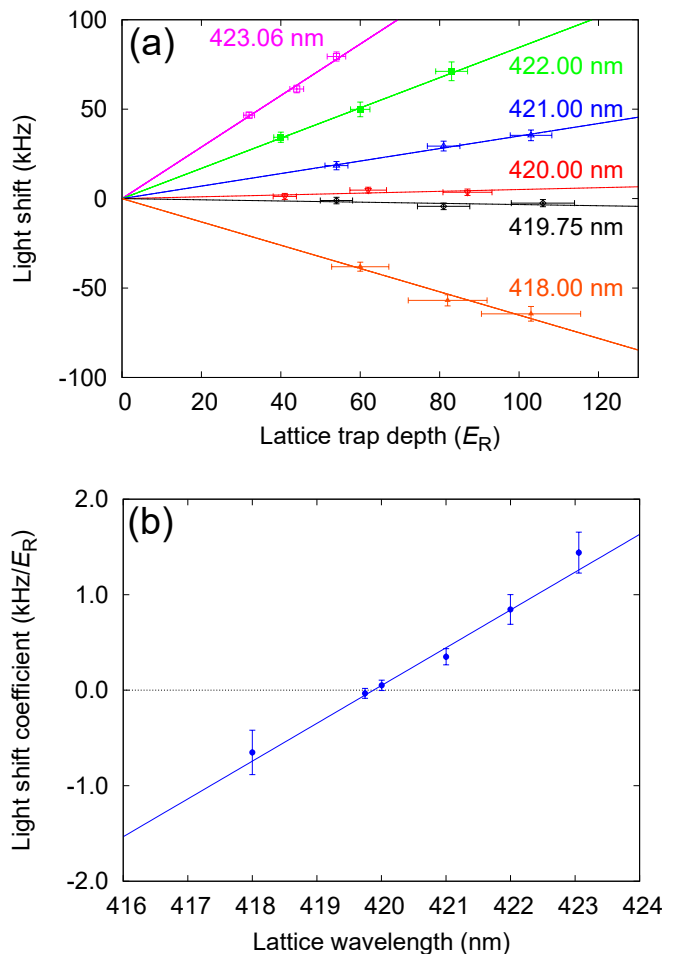


FIG. 5. (a) Light shifts for six lattice wavelengths at three lattice trap depths. At each wavelength the three measured light shifts are linearly fit to extract the light shift coefficient. The slowly drifting frequency offset is subtracted at each wavelength. (b) Light shift coefficient versus lattice wavelength. This gives a magic wavelength of 419.88(14) nm, where the light shift coefficient goes to zero.

and inhibit the 468 nm laser pulses. At each lattice wavelength, the light shifts are linearly fitted and the frequency offset of each linear fit is subtracted so that all fits intersect at zero trap depth. The typical frequency drift of the clock laser is less than 1.5 kHz in 30 minutes, the time required for light shift measurements at a single lattice wavelength. The error bars in Fig. 5(a) include the statistical uncertainty of the fit to the center of the clock excitation spectrum and the frequency drift of the clock laser. The lattice wavelength is measured by a calibrated wavemeter with an uncertainty much less than 1 ppm.

Figure 5(b) shows the lattice light shift per lattice-photon recoil-energy E_R , as a function of the lattice wavelength λ_L . The error bars are the 1σ fit uncertainties from Fig. 5(a). With a linear fit to all the light shift coefficients, the magic wavelength for the $^1S_0 - ^3P_0$ tran-

TABLE I. Contributions to static and dynamic polarizabilities (in a.u.) at the theoretical value of the magic wavelength, 420.1 nm. The experimental transition wavelengths λ (in nm) and theoretical dipole matrix elements D (in a.u.) are given for several leading contributions. The last column is the differential static clock-state polarizability.

State	Contr.	λ	D	α_0	$\alpha_0(\lambda_{\text{magic}})$
$5s^2\ ^1S_0$	$5s5p\ ^3P_1$	326.2	0.158(14)	0.12(2)	0.30(5)
	$5s5p\ ^1P_1$	228.9	3.440(17)	39.62(40)	56.35(56)
	$5s6p\ ^1P_1$	166.9	0.689(14)	1.16(5)	1.38(5)
	Other			0.70(5)	0.78(5)
	Core+vc			4.92(25)	4.92(25)
Total			46.53(47)	63.73(62)	
$5s5p\ ^3P_0$	$5s6s\ ^3S_1$	467.9	1.491(11)	15.22(23)	-63.21(95)
	$5s5d\ ^3D_1$	340.5	2.318(23)	26.76(54)	78.0(1.6)
	$5s7s\ ^3S_1$	308.2	0.433(2)	0.84(1)	1.83(2)
	$5s6d\ ^3D_1$	283.8	1.061(5)	4.67(5)	8.59(9)
	Other			24.00(23)	33.81(46)
	Core+vc			4.70(24)	4.70(24)
Total			76.20(67)	63.7(1.9)	
$\Delta(^3P_0 - ^1S_0)$				29.67(82)	

sition in ^{111}Cd is $\lambda_L = 419.88(14)$ nm (in vacuum). The nonlinearity of the light shift is estimated to be less than 0.2% over a wavelength range of about 10 nm. The experimentally determined magic wavelength agrees with our theoretical prediction of 420.1(7) nm described below, and with a prior semiempirical 420 nm prediction [44]. From the linear fit of the data in Fig. 5(b), the sensitivity of the linear ac Stark shift to the lattice laser wavelength and trap depth is 0.40(2) kHz/ E_R/nm .

Our theoretical calculation of the magic wavelength, and other Cd properties important for clock development, uses a hybrid approach that combines configuration interaction (CI) and an all-order linearized coupled-cluster method [45]. In this CI+all-order method, an effective Hamiltonian is constructed from a coupled-cluster calculation to account for the valence-core (vc), and core-core, correlations. This effective Hamiltonian is subsequently used in the CI calculation of the valence-valence correlations, to obtain the wave functions and the low-lying energy levels by solving the multiparticle relativistic equation $H_{\text{eff}}|\Psi\rangle = E|\Psi\rangle$. The valence contribution to the polarizability comes from the solution of the inhomogeneous equation from a perturbation theory of the valence space [46]. The core polarizability and a small vc correction are calculated using the random-phase approximation. This method yielded high-precision predictions of clock-related properties of Yb [47] and Sr [48]. To estimate the uncertainty of our theoretical predictions, we repeat the calculations with an effective Hamiltonian constructed from second-order perturbation theory (MBPT). The difference between this CI+MBPT and the CI+all-order gives the contributions of the dominant third and higher order terms and serves as estimates of

the theoretical uncertainties. We also compare to calculations for Sr, where several matrix elements are now known with good precision, to make final estimates of our uncertainties.

The contributions to static and dynamic polarizabilities at the theoretical value of the magic wavelength are listed in Table I. Our approach gives the total valence polarizability. Nonetheless, it is insightful to extract several of the dominant contributions, from the lowest states. The experimental transition wavelengths λ (in nm) and dipole matrix elements D (in a.u.) are given for these. The remaining contributions are grouped together as ‘‘Other.’’ While the theoretical and experimental energies agree well [49], it is important to use accurate experimental energies [50] to calculate the dynamical polarizability near the magic wavelength. Because the contributions from the $5s5p\ ^3P_0 - 5s6s\ ^3S_1$ and $5s5p\ ^3P_0 - 5s5d\ ^3D_1$ transitions largely cancel and both resonances are close to the magic wavelength, the small experimental energy corrections can significantly shift the magic wavelength. For consistency, we use experimental energies for the seven contributions listed in Table I. We note that these corrections change the static polarizabilities by much less. We calculate a magic wavelength of 420.1(7)nm, where the uncertainty is the difference between the CI+all-order and CI+MBPT values.

We use the static differential clock polarizability to calculate the static contribution to the blackbody radiation shift $\Delta\nu_{\text{BBR}}^{\text{st}} = -0.255(7)$ Hz. The dynamic correction to the BBR shift is $\Delta\nu_{\text{BBR}}^{\text{dyn}} = -0.45(5)$ mHz, a factor of 330 smaller than that for Sr clocks. This gives a small fractional BBR shift $\Delta\nu_{\text{BBR}}/\nu_0 = -2.83(8) \times 10^{-16}$. The calculations of polarizabilities and the BBR shift are described in more detail in [49].

We calculate the Cd $^1S_0 - ^1S_0$ ground state C_6 coefficient to be 401(8) a.u., following [51]. Using the theoretical $5s5p\ ^1P_1 - 5s^2\ ^1S_0$ matrix element, we predict the 1P_1 lifetime to be 1.500(15) ns. We compared the calculation of $5s5p\ ^1P_1 - 5s^2\ ^1S_0$ matrix element in Cd and Sr [48] and find similar sign and size of the higher-order correlation effects. Due to the similarity of these two cases, confirmed by theory, we use the difference of the Sr value with the experiment (-0.46%) to slightly improve the prediction of the central value of the 1P_1 Cd lifetime. Making the -0.46% adjustment to the Cd matrix element gives lifetimes of 3.424 a.u., or 1.514(15) ns. The predicted 1P_1 lifetime is in agreement with the experimental value of 1.75(0.2) ns [37].

In summary, we have demonstrated two-stage laser cooling that simply and efficiently cools neutral Cd to 6 μK . Loading the ultracold Cd atoms into an optical lattice, we perform Lamb-Dicke spectroscopy on the $^1S_0 - ^3P_0$ clock transition and determine the magic wavelength to be 419.88(14) nm, in agreement with our theoretical prediction of 420.1(7) nm. We calculate the Cd blackbody shift to be $2.83(8) \times 10^{-16}$ at 300 K, in addi-

tion to other properties of Cd. A Cd optical lattice clock therefore can significantly improve the uncertainty originating from BBR, which currently limits the accuracy of Sr and Yb clocks. Assuming a $16\text{-}\mu\text{K}$ -deep lattice, a two-photon-ionization rate is calculated to be 2 mHz for the 3P_0 clock state [35] and the Raman scattering rate to be 0.8 Hz allowing a quality factor of the clock transition of $Q \sim 1.1 \times 10^{15}$. The convenient implementation of deep laser cooling into an optical lattice, the insensitivity to BBR, and abundant nuclear spin 1/2 isotopes make Cd an attractive candidate for compact and transportable optical clocks [52]. Further experimental investigation of higher-order polarizabilities is required to ascertain if Cd clocks can operate with lattice light shift uncertainties less than 10^{-18} .

We thank N. Ohmae, N. Nemitz, K. Hayashida, and M. Takamoto for their comments and technical supports. This work is supported by JST ERATO Grant No. JPMJER1002 10102832 (Japan), by JSPS Grant-in-Aid for Specially Promoted Research Grant No. JP16H06284, by JST-Mirai Program Grant Number JPMJMI18A1, Japan, by the National Science Foundation (KG), and by the USA Office of Naval Research, Grant No. N00014-17-1-2252 (MSS).

-
- [1] B. J. Bloom, T. L. Nicholson, J. R. Williams, S. L. Campbell, M. Bishof, X. Zhang, W. Zhang, S. L. Bromley, and J. Ye, An optical lattice clock with accuracy and stability at the 10^{-18} level, *Nature*, **506**, 71 (2014).
- [2] I. Ushijima, M. Takamoto, M. Das, T. Ohkubo, and H. Katori, Cryogenic optical lattice clocks, *Nat. Photon.* **9**, 185 (2015).
- [3] N. Huntemann, C. Sanner, B. Lipphardt, Chr. Tamm, and E. Peik, Single-Ion Atomic Clock with 3×10^{-18} Systematic Uncertainty, *Phys. Rev. Lett.* **116**, 063001 (2016).
- [4] W. F. McGrew, X. Zhang, R. J. Fasano, S. A. Schäffer, K. Belay, D. Nicolodi, R. C. Brown, N. Hinkley, G. Milani, M. Schioppo, T. H. Yoon, and A. D. Ludlow, Atomic clock performance enabling geodesy below the centimetre level, *Nature* **564**, 87 (2018).
- [5] S. M. Brewer, J.-S. Chen, A. M. Hankin, E. R. Clements, C. W. Chou, D. J. Wineland, D. B. Hume, D. R. Leibbrandt, An $^{27}\text{Al}^+$ quantum-logic clock with systematic uncertainty below 10^{-18} , arXiv:1902.07694 (2019).
- [6] R. Le Targat, L. Lorini, Y. Le Coq, M. Zawada, J. Guéna, M. Abgrall, M. Gurov, P. Rosenbusch, D. G. Rovera, B. Nagórny, R. Gartman, P. G. Westergaard, M. E. Tobar, M. Lours, G. Santarelli, A. Clairon, S. Bize, P. Laurent, P. Lemonde, and J. Lodewyck, Experimental realization of an optical second with strontium lattice clocks, *Nat. Commun.* **4**, 2109 (2013).
- [7] T. Takano, M. Takamoto, I. Ushijima, N. Ohmae, T. Akatsuka, A. Yamaguchi, Y. Kuroishi, H. Munekane, B. Miyahara, and H. Katori, Geopotential measurements with synchronously linked optical lattice clocks, *Nat. Photon.* **10**, 662 (2016).
- [8] J. Grotti, S. Koller, S. Vogt, S. Häfner, U. Sterr, C. Lisdat, H. Denker, C. Voigt, L. Timmen, A. Rolland, F. N. Baynes, H. S. Margolis, M. Zampaolo, P. Thoumany, M. Pizzocaro, B. Rauf, F. Bregolin, A. Tampellini, P. Barbieri, M. Zucco, G. A. Costanzo, C. Clivati, F. Levi, and D. Calonico, Geodesy and metrology with a transportable optical clock, *Nat. Phys.* **14**, 437 (2018).
- [9] N. Huntemann, B. Lipphardt, Chr. Tamm, V. Gerginov, S. Weyers, and E. Peik, Improved Limit on a Temporal Variation of m_p/m_e from Comparisons of Yb^+ and Cs Atomic Clocks, *Phys. Rev. Lett.* **113**, 210802 (2014).
- [10] M. S. Safronova, D. Budker, D. DeMille, D. F. J. Kimball, A. Derevianko, and C. W. Clark, Search for new physics with atoms and molecules, *Rev. Mod. Phys.* **90**, 025008 (2018).
- [11] W. H. Oskay, S. A. Diddams, E. A. Donley, T. M. Fortier, T. P. Heavner, L. Hollberg, W. M. Itano, S. R. Jefferts, M. J. Delaney, K. Kim, F. Levi, T. E. Parker, and J. C. Bergquist, Single-Atom Optical Clock with High Accuracy, *Phys. Rev. Lett.* **97**, 020801 (2006).
- [12] S. R. Jefferts, T. P. Heavner, T. E. Parker, J. H. Shirley, E. A. Donley, N. Ashby, F. Levi, D. Calonico, and G. A. Costanzo, High-Accuracy Measurement of the Blackbody Radiation Frequency Shift of the Ground-State Hyperfine Transition in ^{133}Cs , *Phys. Rev. Lett.* **112**, 050801 (2014).
- [13] N. Nemitz, T. Ohkubo, M. Takamoto, I. Ushijima, M. Das, N. Ohmae, H. Katori, Frequency ratio of Yb and Sr clocks with 5×10^{-17} uncertainty at 150 seconds averaging time, *Nat. Photon.* **10**, 258 (2016).
- [14] J. J. McFerran, L. Yi, S. Mejri, S. Di Manno, W. Zhang, J. Guéna, Y. Le Coq, and S. Bize, Neutral Atom Frequency Reference in the Deep Ultraviolet with Fractional Uncertainty = 5.7×10^{-15} , *Phys. Rev. Lett.* **108**, 183004 (2012).
- [15] K. Yamanaka, N. Ohmae, I. Ushijima, M. Takamoto, and H. Katori, Frequency Ratio of ^{119}Hg and ^{87}Sr Optical Lattice Clocks beyond the SI Limit, *Phys. Rev. Lett.* **114**, 230801 (2015).
- [16] A. P. Kulosa, D. Fim, K. H. Zipfel, S. Rühmann, S. Sauer, N. Jha, K. Gibble, W. Ertmer, E. M. Rasel, M. S. Safronova, U. I. Safronova, and S. G. Porsev, Towards a Mg Lattice Clock: Observation of the $^1S_0\text{-}^3P_0$ Transition and Determination of the Magic Wavelength, *Phys. Rev. Lett.* **115**, 240801 (2015).
- [17] D. Sukachev, S. Fedorov, I. Tolstikhina, D. Tregubov, E. Kalganova, G. Vishnyakova, A. Golovizin, N. Kolachevsky, K. Khabarova, and V. Sorokin, Inner-shell magnetic dipole transition in Tm atoms: A candidate for optical lattice clocks, *Phys. Rev. A* **94**, 022512 (2016).
- [18] A. Golovizin, E. Fedorova, D. Tregubov, D. Sukachev, K. Khabarova, V. Sorokin, and N. Kolachevsky, Inner-shell clock transition in atomic thulium with a small blackbody radiation shift, *Nat. Commun.* **10**, 1724 (2019).
- [19] Y. Kaneda, J. M. Yarborough, Y. Merzlyak, A. Yamaguchi, K. Hayashida, N. Ohmae, and H. Katori, Continuous-wave, single-frequency 229 nm laser source for laser cooling of cadmium atoms, *Opt. Lett.* **41**, 705 (2016).
- [20] C. W. Chou, D. B. Hume, J. C. J. Koelemeij, D. J. Wineland, and T. Rosenband, Frequency Comparison of Two High-Accuracy Al^+ Optical Clocks, *Phys. Rev. Lett.* **104**, 070802 (2010).
- [21] N. Ohtsubo, Y. Li, K. Matsubara, T. Ido, and K. Hayasaka, Frequency measurement of the clock transi-

- tion of an indium ion sympathetically-cooled in a linear trap, *Opt. Express* **25**, 11725 (2017).
- [22] K. J. Arnold, R. Kaewuam, A. Roy, T. R. Tan, and M. D. Barrett, Blackbody radiation shift assessment for a lutetium ion clock, *Nat. Commun.* **9**, 1650 (2018).
- [23] E. Peik and Chr. Tamm, Nuclear laser spectroscopy of the 3.5 eV transition in Th-229, *Europhys. Lett.* **61**, 181 (2003).
- [24] C. J. Campbell, A. G. Radnaev, A. Kuzmich, V. A. Dzuba, V. V. Flambaum, and A. Derevianko, Single-Ion Nuclear Clock for Metrology at the 19th Decimal Place, *Phys. Rev. Lett.* **108**, 120802 (2012).
- [25] V. A. Dzuba, V. V. Flambaum, and H. Katori, Optical clock sensitive to variations of the fine-structure constant based on the Ho^{14+} ion, *Phys. Rev. A* **91**, 022119 (2015).
- [26] M. G. Kozlov, M. S. Safronova, J. R. C. López-Urrutia, and P. O. Schmidt, Highly charged ions: Optical clocks and applications in fundamental physics, *Rev. Mod. Phys.* **90**, 045005 (2018).
- [27] R. H. Garstang, Hyperfine Structure and Intercombination Line Intensities in the Spectra of Magnesium, Zinc, Cadmium, and Mercury, *J. Opt. Soc. Am.* **52**, 845 (1962).
- [28] W. E. v.d. Veer, D. Ph. v.d. Blonk, A. Dönszelmann, and C. Snoek, Lifetime measurements in neutral cadmium and copper, *Proceedings of the 3rd International Colloquium of the Royal Netherlands Academy of Arts and Sciences (1989)*, Amsterdam, 1990, edited by J. E. Hansen, p.176.
- [29] P. Masłowski, K. Bielska, A. Cygan, J. Domysławska, D. Lisak, R. Ciuryło, A. Bielski, and R. S. Trawiński, The hyperfine and isotope structure of the Cd intercombination line - revisited, *Eur. Phys. J. D* **51**, 295 (2009).
- [30] I. Ushijima, M. Takamoto, and H. Katori, Operational Magic Intensity for Sr Optical Lattice Clocks, *Phys. Rev. Lett.* **121**, 263202 (2018).
- [31] T. Walker, D. Sesko, and C. Wieman, Collective behavior of optically trapped neutral atoms, *Phys. Rev. Lett.* **64**, 408 (1990).
- [32] P. M. Duarte, R. A. Hart, J. M. Hitchcock, T. A. Corcovilos, T.-L. Yang, A. Reed, and R. G. Hulet, All-optical production of a lithium quantum gas using narrow-line laser cooling, *Phys. Rev. A* **84**, 061406(R) (2011).
- [33] D. C. McKay, D. Jervis, D. J. Fine, J. W. Simpson-Porco, G. J. A. Edge, and J. H. Thywissen, Low-temperature high-density magneto-optical trapping of potassium using the open $4S \rightarrow 5P$ transition at 405 nm, *Phys. Rev. A* **84**, 063420 (2011).
- [34] S. Stellmer, B. Pasquiou, R. Grimm, and F. Schreck, Laser Cooling to Quantum Degeneracy, *Phys. Rev. Lett.* **110**, 263003 (2013).
- [35] V. D. Ovsiannikov, S. I. Marmo, V. G. Palchikov, and H. Katori, Higher-order effects on the precision of clocks of neutral atoms in optical lattices, *Phys. Rev. A* **93**, 043420 (2016).
- [36] J. Mitroy, M. S. Safronova, and C. W. Clark, Theory and applications of atomic and ionic polarizabilities, *J. Phys. B: At. Mol. Opt. Phys.* **43**, 202001 (2010).
- [37] H. L. Xu, A. Persson, S. Svanberg, K. Blagoev, G. Malcheva, V. Pentchev, E. Biémont, J. Campos, M. Ortiz, and R. Mayo, Radiative lifetime and transition probabilities in Cd I and Cd II, *Phys. Rev. A* **70**, 042508 (2004).
- [38] K.-A. Brickman, M.-S. Chang, M. Acton, A. Chew, D. Matsukevich, P. C. Haljan, V. S. Bagnato, and C. Monroe, Magneto-optical trapping of cadmium, *Phys. Rev. A* **76**, 043411 (2007).
- [39] H. Katori, T. Ido, Y. Isoya, M. Kuwata-Gonokami, Magneto-Optical Trapping and Cooling of Strontium Atoms down to the Photon Recoil Temperature, *Phys. Rev. Lett.* **82**, 1116 (1999).
- [40] P. D. Lett, W. D. Phillips, S. L. Rolston, C. E. Tanner, R. N. Watts, and C. I. Westbrook, Optical molasses, *J. Opt. Soc. Am. B* **6**, 2084 (1989).
- [41] W. Nagourney, J. Sandberg, and H. Dehmelt, Shelved optical electron amplifier: Observation of quantum jumps, *Phys. Rev. Lett.* **56**, 2797 (1986).
- [42] M. Takamoto and H. Katori, Spectroscopy of the $^1S_0-^3P_0$ Clock Transition of ^{87}Sr in an Optical Lattice, *Phys. Rev. Lett.* **91**, 223001 (2003).
- [43] S. Blatt, J. W. Thomsen, G. K. Campbell, A. D. Ludlow, M. D. Swallows, M. J. Martin, M. M. Boyd, and J. Ye, Rabi spectroscopy and excitation inhomogeneity in a one-dimensional optical lattice clock, *Phys. Rev. A* **80**, 052703 (2009).
- [44] A. Ye and G. Wang, Dipole polarizabilities of $ns^2\ ^1S_0$ and $nsnp\ ^3P_0$ states and relevant magic wavelengths of group-IIB atoms, *Phys. Rev. A* **78**, 014502 (2008).
- [45] M. S. Safronova, M. G. Kozlov, W. R. Johnson and D. Jiang, Development of a configuration-interaction plus all-order method for atomic calculations, *Phys. Rev. A* **80**, 012516 (2009).
- [46] S. G. Porsev, Yu. G. Rakhлина, and M. G. Kozlov, Electric-dipole amplitudes, lifetimes, and polarizabilities of the low-lying levels of atomic ytterbium, *Phys. Rev. A* **60**, 2781 (1999).
- [47] M. S. Safronova, S. G. Porsev, and C. W. Clark, Ytterbium in Quantum Gases and Atomic Clocks: van der Waals Interactions and Blackbody Shifts, *Phys. Rev. Lett.* **109**, 230802 (2012).
- [48] M. S. Safronova, S. G. Porsev, U. I. Safronova, M. G. Kozlov, and C. W. Clark, Blackbody-radiation shift in the Sr optical atomic clock, *Phys. Rev. A* **87**, 012509 (2013).
- [49] See Supplemental Material at URL for details of the theoretical calculations, which includes Ref. [53].
- [50] A. Kramida, Yu. Ralchenko, J. Reader, and NIST ASD Team (2018). NIST Atomic Spectra Database (version 5.6.1), <https://physics.nist.gov/asd>. National Institute of Standards and Technology, Gaithersburg, MD. DOI: <https://doi.org/10.18434/T4W30F>.
- [51] S. G. Porsev, M. S. Safronova, and C. W. Clark, Relativistic calculations of C_6 and C_8 coefficients for strontium dimers, *Phys. Rev. A* **90**, 052715 (2014).
- [52] S. B. Koller, J. Grotti, St. Vogt, A. Al-Masoudi, S. Dörscher, S. Häfner, U. Sterr, and Ch. Lisdat, Transportable Optical Lattice Clock with 7×10^{-17} Uncertainty, *Phys. Rev. Lett.* **118**, 073601 (2017).
- [53] S. G. Porsev and A. Derevianko, Multipolar theory of blackbody radiation shift of atomic energy levels and its implications for optical lattice clocks, *Phys. Rev. A* **74**, 020502(R) (2006).

Supplemental Material

Calculations of Cd polarizabilities, magic wavelength and blackbody radiation shift

A. Yamaguchi,^{1,2} M. S. Safronova,^{3,4} K. Gibble,^{1,5} and H. Katori^{1,2,6}¹Quantum Metrology Laboratory, RIKEN, Wako, Saitama 351-0198, Japan²Space-Time Engineering Research Team, RIKEN, Wako, Saitama 351-0198, Japan³Department of Physics and Astronomy, University of Delaware, Newark, Delaware 19716, USA⁴Joint Quantum Institute, NIST and the University of Maryland, College Park, Maryland 20742, USA⁵Department of Physics, The Pennsylvania State University, University Park, Pennsylvania 16802, USA⁶Department of Applied Physics, Graduate School of Engineering,
The University of Tokyo, Bunkyo-ku, Tokyo 113-8656, Japan

In both our CI+all-order and CI+MBPT methods, we calculate the valence contribution to the polarizability for a state v , with total angular momentum J and projection M , from the solution of the inhomogeneous equation from a perturbation theory of the valence space [1]

$$(E_v - H_{\text{eff}})|\Psi(v, M')\rangle = D_{\text{eff},q}|\Psi_0(v, J, M)\rangle. \quad (1)$$

The effective Hamiltonian H_{eff} includes the all-order corrections, and the effective dipole operator D_{eff} includes random phase approximation (RPA) corrections.

The dominant contributions from the lowest states is given by the sum-over-states expression for the valence static polarizability $\alpha_0(\omega)$:

$$\alpha_0(\omega) = \frac{2}{3(2J+1)} \sum_k \frac{\Delta E \langle k || D || v \rangle^2}{\Delta E^2 - \omega^2}, \quad (2)$$

where $\Delta E = E_k - E_v$ and the sum is over intermediate states k with allowed electric-dipole transitions [2]. These contributions are listed separately in Table I for both the CI+MPBT and CI+all-order calculations. The remaining contributions listed in the rows ‘‘Other’’ are the difference of the total value obtained by solving the inhomogeneous equation above and the sum of the contributions calculated with the sum-over-state formula (2). The core polarizability and a small vc correction are calculated using RPA.

We also list the theoretical and experimental energies [3] and their differences in Table I, along with theoretical dipole matrix elements, and contributions to the polarizability. The results from *ab initio* calculations of the dominant terms are in column ‘‘A’’. To improve the accuracy, we recalculated these contributions using the experimental energies, which is particularly important for the dynamic polarizabilities. These are shown in column ‘‘B’’ and are used as the final values. Since the magic wavelength lies between the $5s5p \ ^3P_0 - 5s6s \ ^3S_1$ and $5s5p \ ^3P_0 - 5s5d \ ^3D_1$ resonance, these terms contribute with a opposite signs. As a result, even a 1% change of the experimental energy leads to large changes in the total, and significantly shifts the calculated magic wavelength, for which $\alpha_0(^1S_0)(\lambda_{\text{magic}}) = \alpha_0(^3P_0)(\lambda_{\text{magic}})$. Using experimental energies shifts the CI+all-order magic

wavelength from 425.0 nm to the final value of 420.1 nm, and for CI+MBPT, which gives less accurate energies, it shifts from 428.6 nm to a final value of 419.4 nm. We take the difference of final CI+all-order and CI+MBPT values as an uncertainty, yielding $\lambda_{\text{magic}} = 420.1(7)$ nm.

The blackbody radiation shift (BBR) of state v can be expressed in terms of the static polarizability $\alpha_0(0)$ as [4]

$$\Delta E_v = -\frac{2}{15}(\alpha\pi)^3(k_B T)^4 \alpha_0(0)(1 + \eta), \quad (3)$$

where the first term describes the static contribution and the second gives the dynamic contribution to the BBR shift. The quantity η is approximated by [4]

$$\eta = \eta_1 + \eta_2 + \eta_3 = \frac{80}{63(2J+1)} \frac{\pi^2}{\alpha_0(0)k_B T} \times \sum_k \frac{|\langle k || D || v \rangle|^2}{y_k^3} \left(1 + \frac{21\pi^2}{5y_k^2} + \frac{336\pi^4}{11y_k^4} \right), \quad (4)$$

where $y_k = (E_k - E_v)/(k_B T)$.

Table II lists the contributions to η for the Cd clock states. The contributions of η_2 and η_3 are currently negligible. We estimate the contribution of the higher states to $\eta(^3P_0)$, listed as ‘‘Other,’’ using the scaling of the higher state contributions to the 3P_0 polarizability. We use the final values of the static polarizabilities $\alpha_0(^1S_0) = 46.53(47)$ a.u. and $\alpha_0(^3P_0) = 76.20(67)$ a.u., given in Table I, to calculate the static contribution to the BBR shift, $\Delta\nu_{\text{BBR}}^{\text{st}} = -0.255(7)$ Hz. The dynamic correction is $\Delta\nu_{\text{BBR}}^{\text{dyn}} = -0.45(5)$ mHz, giving a total BBR shift of $-0.256(7)$ Hz, fractionally $\Delta\nu^{\text{BBR}}/\nu_0 = -2.83(8) \times 10^{-16}$ at 300K.

-
- [1] S. G. Porsev, Yu. G. Rakhlina, and M. G. Kozlov, Electric-dipole amplitudes, lifetimes, and polarizabilities of the low-lying levels of atomic ytterbium, *Phys. Rev. A* **60**, 2781 (1999).
- [2] J. Mitroy, M. S. Safronova, and C. W. Clark, Theory and applications of atomic and ionic polarizabilities, *J. Phys. B* **43**, 202001 (2010).

- [3] A. Kramida, Yu. Ralchenko, J. Reader, and NIST ASD Team (2018). NIST Atomic Spectra Database (version 5.6.1), <https://physics.nist.gov/asd>. National Institute of Standards and Technology, Gaithersburg, MD. DOI: <https://doi.org/10.18434/T4W30F>.
- [4] S. G. Porsev and A. Derevianko, Multipolar theory of blackbody radiation shift of atomic energy levels and its implications for optical lattice clocks, *Phys. Rev. A* **74**, 020502(R) (2006).

TABLE I. Results of CI+MBPT and CI+all-order calculations. Contributions to static and dynamic polarizabilities (in a.u.) at the theoretical value of the magic wavelength, $\lambda_{\text{magic}} = 419.4$ nm for CI+MBPT and $\lambda_{\text{magic}} = 420.1$ nm for CI+all-order calculations, respectively. The experimental and theoretical energies, in cm^{-1} , and theoretical dipole matrix elements D in a.u. are given for several contributions. The difference between the experimental and theoretical energies are given in the row labeled “Diff.,” in cm^{-1} . The dominant terms are in columns A and B , calculated using theoretical and experimental energies respectively.

State	Contr.	Energy		Diff.	D	α_0		$\alpha_0(\lambda_{\text{magic}})$		
		Theory	Expt.			A	B	A	B	
CI+MBPT calculations										
$5s^2 \ ^1S_0$	$5s5p \ ^3P_1$	31855	30656	-1199	0.172	0.14	0.14	0.31	0.36	
	$5s5p \ ^1P_1$	44099	43692	-407	3.426	38.94	39.30	55.02	55.97	
	$5s6p \ ^1P_1$	60595	59907	-687	0.675	1.10	1.11	1.30	1.32	
	Other					0.66	0.66	0.73	0.73	
	Core+vc					4.92	4.92	4.92	4.92	
	Total					45.76	46.14	62.29	63.30	
$5s5p \ ^3P_0$	$5s6s \ ^3S_1$	20883	21370	487	1.502	15.81	15.45	-52.06	-63.08	
	$5s5d \ ^3D_1$	28932	29372	440	2.306	26.89	26.49	83.82	77.68	
	$5s7s \ ^3S_1$	31947	32449	502	0.432	0.86	0.84	1.93	1.83	
	$5s6d \ ^3D_1$	34756	35239	483	1.062	4.74	4.68	8.96	8.63	
	Other					23.77	23.77	33.38	33.38	
	Total					76.77	75.93	80.74	63.15	
CI+all-order calculations										
$5s^2 \ ^1S_0$	$5s5p \ ^3P_1$	30969	30656	-312	0.158	0.12	0.12(2)	0.29	0.30(5)	
	$5s5p \ ^1P_1$	43715	43692	-22	3.440	39.60	39.62(40)	56.29	56.35(56)	
	$5s6p \ ^1P_1$	59969	59907	-62	0.689	1.16	1.16(5)	1.37	1.38(5)	
	Other					0.70	0.70(5)	0.78	0.78(5)	
	Core+vc					4.92	4.92(25)	4.92	4.92(25)	
	Total					46.50	46.53(47)	63.66	63.73(62)	
$5s5p \ ^3P_0$	$5s6s \ ^3S_1$	21133	21370	237	1.491	15.39	15.22(23)	-57.25	-63.21(95)	
	$5s5d \ ^3D_1$	29059	29372	313	2.318	27.05	26.76(54)	82.22	78.0(1.6)	
	$5s7s \ ^3S_1$	32125	32449	324	0.433	0.85	0.84(1)	1.89	1.83(2)	
	$5s6d \ ^3D_1$	34919	35239	321	1.061	4.72	4.67(5)	8.81	8.59(9)	
	Other					24.00	24.00(23)	33.81	33.81(46)	
	Total					76.71	76.20(67)	74.17	63.7(1.9)	

TABLE II. Contributions to the dynamic correction η of the BBR shift at 300K.

State	Contr.	η
$5s^2 \ ^1S_0$	$5s5p \ ^3P_1$	0.000 002
	$5s5p \ ^1P_1$	0.000 365(3)
	$5s6p \ ^1P_1$	0.000 006
	Total	0.000 373(3)
$5s5p \ ^3P_0$	$5s6s \ ^3S_1$	0.000 360(5)
	$5s5d \ ^3D_1$	0.000 334(6)
	$5s7s \ ^3S_1$	0.000 009
	$5s6d \ ^3D_1$	0.000 040
	$5s8s \ ^3S_1$	0.000 002
	$5s7d \ ^3D_1$	0.000 013
	$5s9s \ ^3S_1$	0.000 001
	$5s8d \ ^3D_1$	0.000 010
	Other	0.000 148(74)
	Total	0.000 918(74)